Methods 229 (2024) 9–16

Contents lists available at ScienceDirect

Methods

journal homepage: www.elsevier.com/locate/ymeth

MSO-GP: 3-D segmentation of large and complex conjoined tree structures

Arijit De [a,1], Nirmal Das [b,c,1], Punam K. Saha [d], Alejandro Comellas [e], Eric Hoffman [e], Subhadip Basu [b,*,2], Tapabrata Chakraborti [f,g,**,2]

[a] Department of Electronics & Telecommunication Engineering, Jadavpur University, Kolkata, India
[b] Department of Computer Science and Engineering (AIML), Institute of Engineering and Management, Kolkata, India
[c] Department of Computer Science and Engineering, Jadavpur University, Kolkata, India
[d] Department of Electrical and Computer Engineering & Department of Radiology, University of Iowa, Iowa City, IA 52242, USA
[e] Department of Internal Medicine, University of Iowa, Iowa City, USA
[f] Health Sciences Programme, The Alan Turing Institute, London, UK
[g] Department of Medical Physics and Biomedical Engineering, University College London, London, UK

ARTICLE INFO

Keywords:
Multiscale opening
Conjoined trees
Digital topology
Computational biology
3D segmentation
Visual geometry
Morphometry

ABSTRACT

Robust segmentation of large and complex conjoined tree structures in 3-D is a major challenge in computer vision. This is particularly true in computational biology, where we often encounter large data structures in size, but few in number, which poses a hard problem for learning algorithms. We show that merging multiscale opening with geodesic path propagation, can shed new light on this classic machine vision challenge, while circumventing the learning issue by developing an unsupervised visual geometry approach (digital topology/morphometry). The novelty of the proposed MSO-GP method comes from the geodesic path propagation being guided by a skeletonization of the conjoined structure that helps to achieve robust segmentation results in a particularly challenging task in this area, that of artery-vein separation from non-contrast pulmonary computed tomography angiograms. This is an important first step in measuring vascular geometry to then diagnose pulmonary diseases and to develop image-based phenotypes. We first present proof-of-concept results on synthetic data, and then verify the performance on pig lung and human lung data with less segmentation time and user intervention needs than those of the competing methods.

1. Introduction

Though object segmentation from 2D/3D images is a well researched area in computer vision over several decades, it still presents a few tasks with interesting mathematical challenges that are yet to be solved robustly and rigorously. Of course, with the ever-growing popularity of deep learning approaches, some might argue that such emphasis on a mathematically focused solution will soon become a moot point. We would like to counter that especially given the opaque black box like nature of modern deep learning models, the importance of analytical insights into the nature of such classic machine vision problems and mathematical solutions thereof are the need of the hour [1]. In addition to this need for mathematical transparency in model design, is the requirement to preserve performance in situations where we encounter large data structures in size, but few in number, which poses a hard problem for learning algorithms. This is often the case in computational biology, and a prime example of this is robust segmentation of conjoined and complex tree structures, which remains a challenging task to the present day, especially when two or more classes of intertwined branches therein are not colour contrasted and have similar morphology. A classic example of this task is separation of arteries and veins from non-contrast pulmonary computer tomography (CT) angiograms [2]. This is an important first step in measuring vascular geometry to then diagnose pulmonary diseases and to develop image-based phe-

* Corresponding author.
** Corresponding author at: Department of Medical Physics and Biomedical Engineering, University College London, London, UK.
E-mail addresses: arijitde.etce.rs@jadavpuruniversity.in (A. De), nirmal.das@iem.edu.in (N. Das), punam-saha@uiowa.edu (P.K. Saha), alejandro-comellas@uiowa.edu (A. Comellas), eric-hoffman@uiowa.edu (E. Hoffman), subhadip.basu@jadavpuruniversity.in (S. Basu), tchakraborty@turing.ac.uk, t.chakraborty@ucl.ac.uk (T. Chakraborti).
[1] AD and ND are joint first authors with equal contributions.
[2] TC and SB are joint corresponding/senior authors. TC is supported by the Turing-Roche Strategic Partnership.

https://doi.org/10.1016/j.ymeth.2024.05.016
Received 22 October 2023; Received in revised form 3 May 2024; Accepted 29 May 2024
Available online 3 June 2024

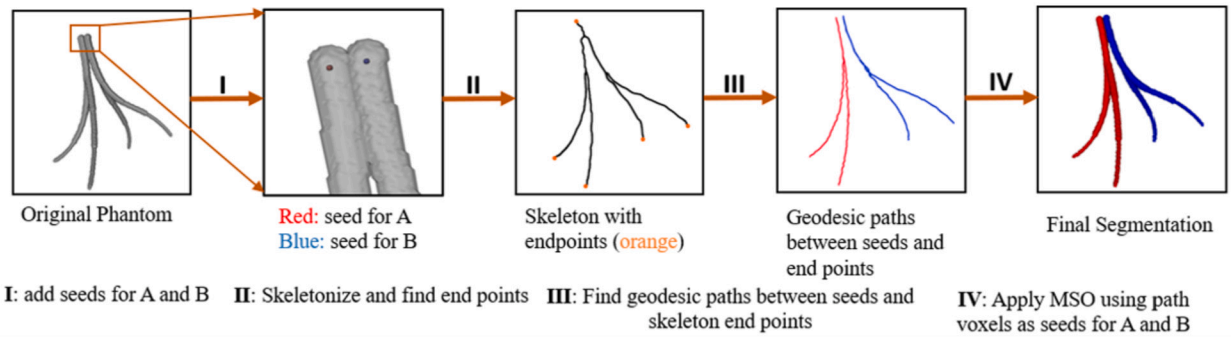

Fig. 1. MSO-GP steps for separation of conjoined structures in iso-intensity space.

notype. There exist some prior methods in the space of artery-vein segmentation from lung CT angiograms, a sizeable proportion of the early approaches being focused on improvised image acquisition techniques. A detail discussion on the shortcomings of such "pre-processing" based approaches has been reported in [3]. There have also been some segmentation work of complex A/V tree structures on MR images, but they primarily depend on the intensity variation at the fusion location which is not true for non-contrast low resolution pulmonary CT images [3][4]. The works reported in [5,6] classified pulmonary arteries and veins, but these use multi-slice CT which result in higher contrast, while the present method seeks to provide robust performance even in the case of non-contrast CT image.

Recently deep learning models are also being used for vessel like tree structure segmentation from images of different modalities [7,8]. In [9], an edge-reinforced deep learning model was proposed to segment 3-D vessel structures from two cerebrovascular and two nerve datasets. In an encoder-decoder network, a reverse edge attention module and an edge-reinforced optimization loss were introduced to better preserve the edge information leading to better segmentation output. The work in [10] introduced DeepVesselNet to overcome challenges like high memory requirements and class imbalance problems that are common in vessel segmentation task. The method was validated on clinical MRA of human brain and microscopic CTA of rat brain. A 3D CNN was proposed for rapid vessel segmentation and reconstruction from head and neck CTA in [11]. The model was trained and tested with 18,766 head and neck CTA scans from 5 tertiary hospitals in China. Although the above works were designed for vessel segmentation, they did not address the problem of conjoined structure segmentation in iso-intensity space. The above mentioned deep models used intensity values to achieve segmentation. The works in [12] and [13] specifically addressed the problem of pulmonary artery-vein separation from non-contrast CT. In [12], the authors presented a CNN-based method to segment the pulmonary airway, artery, and vein from non-contrast CT images. They introduced a feature recalibration module to better use the features learned from the neural networks and an attention distillation module to reinforce representation learning of tubular objects. Lung context map and distance transform map were incorporated as shape prior for better artery-vein differentiation capacity. The work reported in [13], proposed an integrative solution for the automatic identification of pulmonary arteries and veins from non-contrast chest CT images. First, the larger extrapulmonary arteries and veins are extracted using 3-D CNN, and then a computational differential geometry-based method is applied in the second phase to extract the prominent intrapulmonary vessels, without separating arteries and veins. The results of the two phases are combined. Starting with the extrapulmonary arteries and veins in the combined structure, the intrapulmonary vessels are traced by following their skeletons and differentiated into arteries and veins. This integrative approach limits the requirement of manual labelling of arteries and veins for learning algorithms only to the large extrapulmonary vessels. They used a dataset of 120 chest CT scans acquired on different subjects. However, the dataset and the trained model are not available to compare the results qualitatively/quantitatively. The work used deep learning in the first phase and computational differential geometry in the second phase whereas MSO-GP is an end-to-end digital topology and geometry based approach. In addition to the points above, the general problem in using deep learning methods is the requirement of sufficient expert annotated data. The annotation of pulmonary artery-vein is time-consuming, expensive, and requires expert intervention. MSO-GP is computationally inexpensive, less resource-hungry, and interpretable compared to the general deep learning methods. Moreover, the above-mentioned deep networks are designed for the specific task of pulmonary artery-vein separation, not to address the generic problem of multiscale conjoined object separation in iso-intensity space.

Multi-scale opening (MSO) was introduced to solve this problem in [14] but they assumed that the conjoined objects are locally separable. Their method needs a lot of user interaction in terms of providing separator seeds where objects are not morphologicaly separable. Our method (MSO-GP) takes the core of the multi-scale opening concept, but improves it by employing skeletonization and fuzzy distance transform (FDT) based geodesic path propagation in between which helps to traverse the tree branches and segment more robustly. This novel augmentation helps to segment even those areas of the tree where the artery and vein branches are very similar by morphology also. A schematic illustration of the proposed MSO-GP is presented in Fig. 1. Thus the contribution of the present work is threefold.

1. We revisit the classic computer vision problem of segmenting complex conjoined tree-like visual structures from images with the fresh perspective of modelling the branches as FDT based geodesic paths guided by their skeletons and opening them morphologically in multiple scales with the help of traditional MSO algorithm.
2. The proposed MSO-GP method is unsupervised and non-learning based and is designed to provide robust and mathematically interpretable performance despite scarcity of prior samples and annotations. As a representative task, we demonstrate the method on artery-vein segmentation in non contrast lung computed tomography (CT) angiograms.
3. We provide results on three types of lung CT angiogram data: synthetic generated data, pig lung phantom data and *in vivo* human lung data. MSO-GP yields strong results and outperforms two competing methods. The source code of MSO-GP has been uploaded in a public GitHub repository.

2. Theory and methods

In this section, we present the definitions and notations related to visual representations in 3D digital space, skeletonization, geodesic path (GP) propagation, multi scale opening (MSO) and describe the proposed MSO-GP algorithm. The work falls in the methodological genre of topological geometry and morphometry.

2.1. Basic definitions and notations

A 3D cubic grid is denoted by $\mathcal{Z}^3$ where $\mathcal{Z}$ is the set of positive integers. A voxel is a point on the grid, denoted by (x_1, x_2, x_3) and is a member of $\mathcal{Z}^3$. Two voxels $p = (x_1, x_2, x_3)$ and $q = (y_1, y_2, y_3) \in \mathcal{Z}^3$ are adjacent iff $\{max(|x_i - y_i|) \leq 1 \mid 1 \leq i \leq 3\}$, where $|\bullet|$ means the absolute value. Two adjacent voxels are neighbours and 26 neighbours of a voxel p (not counting itself) are symbolized as $\mathcal{N}^*(p)$ in a $3 \times 3 \times 3$ cubic grid neighbourhood. A set of neighbouring voxels can constitute a fuzzy object $\mathbb{O}$ defined as $\{(p, \mu_{\mathbb{O}}(p)) | p \in \mathcal{Z}^3\}$, where $\mu_{\mathbb{O}} : \mathcal{Z}^3 \to [0, 1]$ is the membership function. The support of $\mathbb{O}$ is the set of all voxels with non-zero membership value i.e. $\Theta(\mathbb{O}) = O = \{p | p \in \mathcal{Z}^3 \text{ and } \mu_{\mathbb{O}}(p) > 0\}$. The fuzzy distance [15] between two voxels $p, q \in \mathcal{Z}^3$ in an object $\mathbb{O}$, expressed as $\omega_{\mathbb{O}}(p, q)$, is the length of one of the shortest paths from p to q, i.e., $\omega_{\mathbb{O}}(p, q) = \min_{\pi \in \mathcal{P}(p,q)} \Pi_{\mathbb{O}}(\pi) | \mathcal{P}(p, q)$ where, $\mathcal{P}(p, q)$ is the set of all paths from p to q. The fuzzy distance transform (FDT) [15] of an object $\mathbb{O}$ is an image, represented as $\{(p, \Omega(p)) | p \in \mathcal{Z}^3\}$, and $\Omega_{\mathbb{O}}(p)$ is the fuzzy distance from the background, $\Omega_{\mathbb{O}}(p) = \min_{q \in \overline{O}} \omega_{\mathbb{O}}(p, q)$, where $\Omega_{\mathbb{O}} : \mathcal{Z}^3 \to \mathbb{R}^+ | \mathbb{R}^+$ is the set of all real numbers including zero. Let $L_{max} \subset O$ be the set of locally deepest voxels i.e. $L_{max} = \{p | p \in O \wedge \forall q \in \mathcal{N}_l(p), \Omega_O(q) \leq \Omega_O(p)\}$ where $\mathcal{N}_l(p)$ denotes the $(2l+1)^3$ neighbourhood of p. So a point may have zero, one or more than one local maxima points in its neighbourhood.

2.2. Fuzzy distance transform based geodesic path propagation

The geodesic path between two points is the minimum cost shortest path. In this article we adopt Dijkstra's algorithm [16] for the shortest path between two 3D points, with the constraint that the shortest path must pass through the nearest local maxima point provided it exists, otherwise it will choose the neighbour with the maximum fuzzy distance transform (FDT) value. A voxel p may have more than one local maxima or may not have any local maxima in $N_l(p)$ i.e. $(2l+1)^3$ neighbourhood of p. We have taken $l = 2$ to avoid noisy local maxima. The geodesic path from a point will pass through its nearest local maxima if that lowers the cost. Let $\mathbb{O}$ be a fuzzy object and $\mathbb{O}_{FDT} = \{(p, \Omega_{\mathbb{O}}(p)) | p \in \mathcal{Z}^3\}$, where $\Omega(p) =$ the fuzzy distance between p and nearest point in $\overline{O}$. First, we evaluate a cost matrix where each point denotes its shortest distance between the source points. We take a set of source points S. The cost matrix can be defined as $C = \{(p, \mu(p)) | p \in \mathcal{Z}^3\}$, where $\mu(p)$ denotes the cost or distance of p to the nearest point in S. The cost or distance between $p \in \mathbb{O}$ and $\mathcal{N}^*(q)$ is given by

$$\mu(p, q) = \frac{\|p - q\|}{\Omega_{\mathbb{O}}(q)} \tag{1}$$

where $\|p - q\|$ is the euclidean norm and $\Omega_{\mathbb{O}}(q)$ denotes the FDT value of q. It is obvious from equation (3) that the least cost path will always pass closer to the medial axis of the object. While calculating the C matrix $\forall p \in \mathbb{O}$, we can store a $q \in \mathcal{N}^*(p)$ for which $\mu(p, q)$ is minimum. With the help of this least cost neighbour, we can trace the path from any $p \in \mathbb{O}$ to the nearest $q \in S$. This is the geodesic path and we present an algorithm (see Algorithm 1) to find the geodesic path from any $p \in \mathbb{O}$ to $q \in S$ by computing the cost matrix, C.

2.3. Proposed MSO-GP: multi-scale opening with geodesic path model

In the proposed MSO-GP algorithm, we first find out the skeleton of the object. For a object $\mathbb{O}$, the skeleton of the object is defined as:

$$S_{\mathbb{O}} = \{x \in \mathbb{O} | \exists b_1, b_2 \in \partial O, b_1 \neq b_2, \|x - b_1\| = \|x - b_2\|\} \tag{2}$$

where b_1, $b_2 \in \partial O$ are boundary points [17]. We find out the end points of $S_{\mathbb{O}}$ using the methods introduced in [18]. The set of end points of $S_{\mathbb{O}}$ is denoted as $E(S_{\mathbb{O}})$. Let the object $\mathbb{O}$ consist of two conjoined fuzzy objects A and B. The region acquired by A is denoted as R_A and the region acquired by B is denoted as R_B. To start the MSO-GP algorithm three sets of seed points are taken, S_A:=set of seeds for A, S_B:=set of seeds for B, and S_S: the set of separator seeds. We consider S_A, S_B as source points and $\forall x \in E(S_{\mathbb{O}})$ as the end points to run the MSO-GP algorithm. The end points which connect to the points in S_A create the geodesic paths inside A and the end points which connect to the points in S_B create geodesic paths inside B. The set of all paths inside A is denoted as ρ_A and the set of all paths inside B is denoted as ρ_B. ρ_A and ρ_B are mutually exclusive. All the path points of a path in ρ_A are added with S_A and all the path points of a path ρ_B are added with S_B. We get a new set of seed points $S'_A = S_A + \rho_A$ and $S'_B = S_B + \rho_B$ for object A and B respectively. With the sets of seed points S'_A, S'_B, MSO-GP follows the usual path of MSO algorithm to disconnect A and B.

Algorithm 1: GP Algorithm.

Input:
$\mathbb{O}$: An fuzzy object in $\mathcal{Z}^3$
S: Set of source points
E: Set of end points
X: Set of object voxels
Q: A queue
C: An image where each voxel value represents its distance from the nearest seed
NN: An image where each voxel stores its nearest source points
$\mu(p, q)$: Distance of the link between p, q
Initialize:
$\forall p \in X$, $C(p) = \infty$, $NN(p) = NULL$
$\forall p \in S$, $C(p) = 0$, $NN(p) = p$
PUSH p in Q
while Q *is non empty* **do**
  POP p from Q
  $\forall q \in \mathcal{N}^*(p) \cap X$,
  if $C(q) > C(p) + \mu(p, q)$ **then**
    $C(q) = C(p) + \mu(p, q)$
    $NN(q) = NN(p)$
    PUSH q in Q
  end
end
for *any end point* $p \in E$ **do**
  while $q \notin S$ **do**
    Initiate a path $\pi = p$ and set $q = p$ for $q \in \mathcal{N}^*(p)$
    if $q \in X$ **then**
      $q = NN_q$
      Append q in π
    end
  end
end

Fuzzy morpho-connectivity strength of a path $\pi = < p_1, p_2, \ldots, p_l >$ in a fuzzy object $\mathbb{O}$, expressed as $\Gamma(\pi)$, is the minimum FDT value along the path. $\Gamma_{\mathbb{O}}(\pi) = \min_{1 \leq i \leq l} \Omega(p_i)$ Fuzzy morpho-connectivity between two voxels $p, q \in \mathcal{Z}^3$, is the strength of the strongest morphological path between them. Fuzzy morpho-connectivity strength between the two voxels can be denoted by $\gamma_{\mathbb{O}}(p, q) = \max_{\pi \in \mathcal{P}(p,q)} \Gamma_{\mathbb{O}}(\pi)$. Optimum erosion of a fuzzy object A represented by the set of seed voxels S'_A with respect to its co-object B, represented by the set of seed voxels S'_B and a set of common separator S_S, is the set of all voxels p such that there exists an erosion scale that disconnects p from B while leaving it connected to A, i.e.

$$R_{A,0} = \left\{ p \Big| \max_{a \in S'_A} \gamma_{A,0}(a, p) > \max_{b \in S'_B} \gamma_{B,0}(b, p) \right\} \tag{3}$$

where the fuzzy morpho-connectivity functions $\gamma_{A,0}$ and $\gamma_{B,0}$ are defined from the FDT maps $\Omega_{A,0}$ and $\Omega_{B,0}$ respectively. The optimum erosion $R_{B,0}$ of the object B is defined similarly. As the fuzzy morpho-connectivity strength depends on the FDT value of the voxels along the path, hence in optimum erosion the region through which artery passes plays an important role in the segmentation process, specifically, in iso-intensity regions. As two separated regions only capture an eroded version of the target object, hence constraint dilation has been used to further improve the data. Constrained dilation of $R_{A,0}$ with respect to

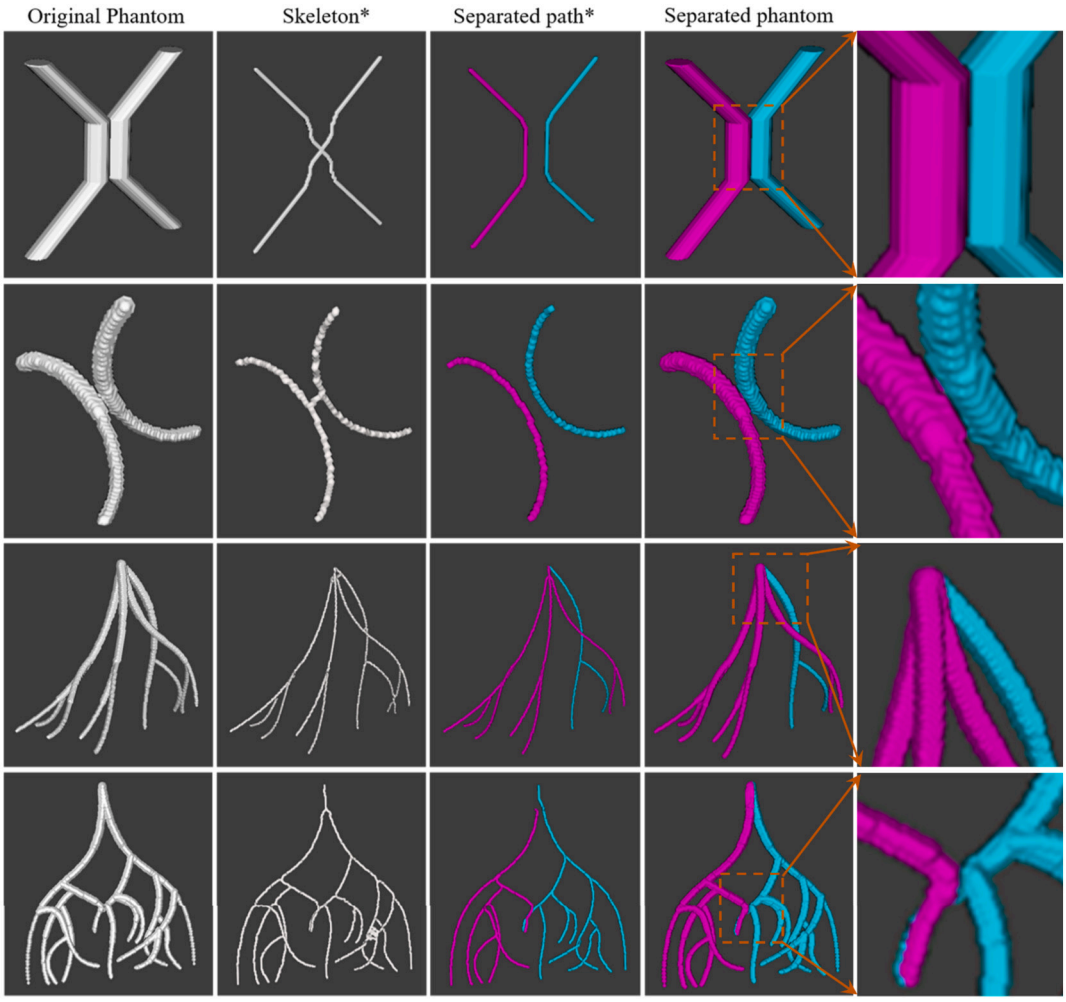

Fig. 2. Separation of conjoined mathematical/synthetic phantoms using the proposed MSO-GP algorithm. First original phantom image is shown, followed by skeleton, separated geodesic paths, final separated phantom, and zoomed in view of the selected ROI from the final separated image. (*Skeletons and geodesic paths are dilated by 3x3x3 mask for better visualization here in the paper using ITK-SNAP software [19].)

its co-object $R_{B,0}$ within the fuzzy object $\mathbb{O}$, denoted as $M_{A,0}$ is the set of all voxels $p \in \mathcal{N}_{\mathbb{O}}\left(R_{A,0}\right)$ which are strictly closer to $R_{A,0}$ than $R_{B,0}$ i.e.,

$$M_{A,0} = \{p \mid p \in \mathcal{N}_{\mathbb{O}}(R_{A,0}) \wedge min_{a \in R_{A,0}} \omega_{\mathbb{O}}(a,p) < min_{b \in R_{B,0}} \omega_{\mathbb{O}}(b,p)\} \tag{4}$$

where $\mathcal{N}_{\mathbb{O}}(R_{A,0})$ is morphological neighbourhood of a set of voxels $p \in O$ such that there exists a $q \in R_{A,0}$ for which $\omega_{\mathbb{O}}(p,q) < \Omega_{\mathbb{O}}(q)$ and p is connected to q by a path π of monotonically increasing FDT values.

The developed method connects the vessel seed points by the FDT based geodesic path. Therefore, the number of pure vessel points increase significantly in the iso-intensity space with minimal user intervention. If required, additional manual seeds may be introduced to correct the intermediate points on the path. The algorithm starts from the initial set of vessel points generated by the FDT based geodesic path points. The algorithm separates two target objects at a specific scale and iteratively propagates to finer scales. For each of the two objects, we set the FDT values to zero over the region currently acquired by its rival object. It puts a hypothetical wall at the boundary of each object separated in the previous iteration stopping paths from one object to run through the territory already acquired by the rival object. Specifically, after each iteration, the FDT image of object A is updated as follows:

$$\Omega_{A,i}(p) = \begin{cases} 0, & if \quad p \in \mathcal{N}_{\mathbb{O}}\left(R_{B,i-1}\right) - M_{A,i-1} \\ \Omega_{A,i-1}(p), & otherwise \end{cases} \tag{5}$$

The FDT map of the other object is updated similarly. The seed voxels for the two objects are replaced by $M_{A,i-1}$ and $M_{B,i-1}$, respectively. With this setup, the algorithm enters into the next iteration and the morphological separation of $M_{A,i}$ and $M_{B,i}$ is derived using the equations above.

3. Experiments and results

We have evaluated the performance of proposed MSO-GP algorithm in the context of a challenging segmentation task i.e., segmentation of large and complex multiscale conjoined objects. The algorithm is validated on three types of data 1) synthetic phantoms, 2) pig lung phantoms, and 3) human lung CT image. The mathematical or synthetic phantoms were generated using a 2D GUI [20]. The GUI takes control points form the user and draws a 3D Bezier curve using those control points. Spheres of varying radius are drawn at each point of the Bezier curves to create the synthetic phantoms. The generated phantoms mimic pulmonary artery-vein (A/V) trees and fusion of vessels in iso-intensity space. The user can load A/V trees on the GUI and take the control points with reference to the original A/V tree to create more complex and realistic vessel phantoms. Fig. 2 shows the segmentation performance of our MSO-GP algorithm on four mathematical phantoms. We can see that the skeletons of the conjoined phantoms are connected but the geodesic paths are disconnected and using these geodesic path points as initial seed points and applying the proposed MSO-GP method,

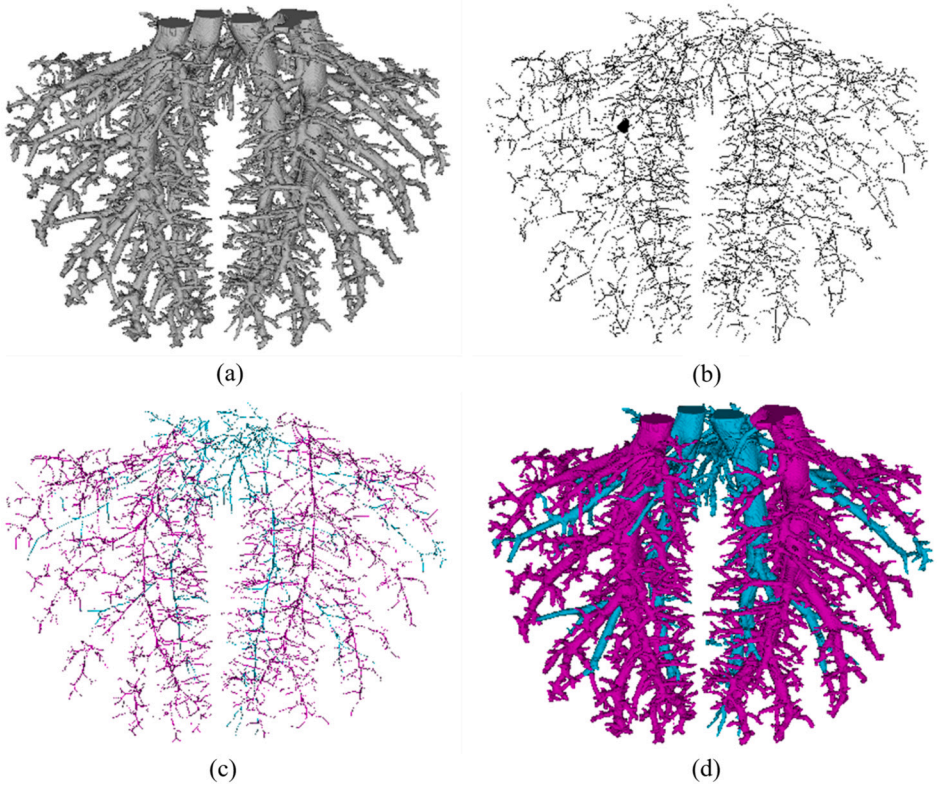

Fig. 3. Separation of artery-vein in Pig Lung phantom (a) Original Pig Lung phantom (b) Skeleton of the phantom (c) Geodesic paths between user given artery and vein seeds and skeletal end points. (d) Final A/V segmentation.

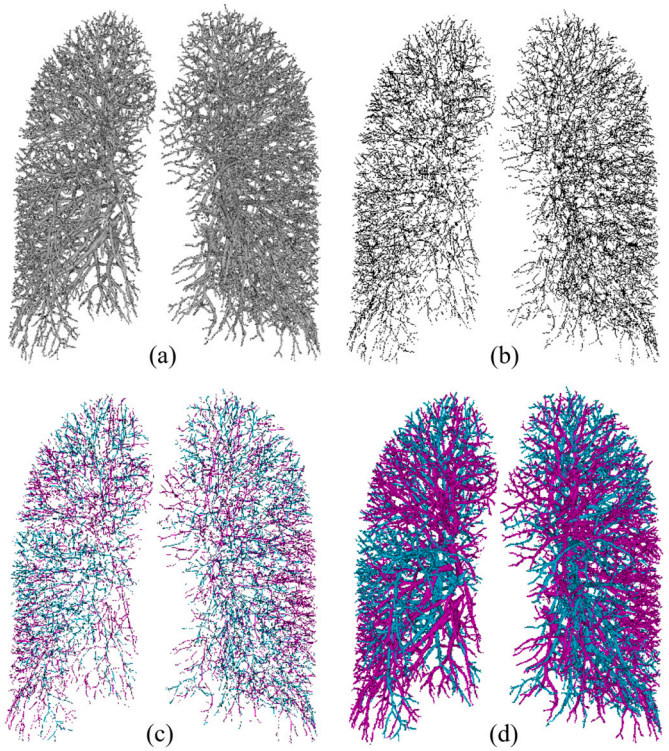

Fig. 4. Separation of artery and vein in A/V tree extracted from human lung CT. (a) Original A/V tree, (b) skeleton of the A/V tree, (c) Geodesic paths between user given artery and vein seeds and skeletal end points, (d) Final A/V segmentation.

we get the final separated phantom. Results of application of the MSO-GP algorithm to a CT image of a pig lung cast phantom are presented in Fig. 3. The reader is encouraged to refer to [2] for details of clinical preparation of the pig lung phantom and extraction of the A/V tree, generated at the Advanced Pulmonary Physiomic Imaging Laboratory (APPIL), University of Iowa, USA. For the pig lung phantom shown in Fig. 3, with voxel dimension of $512 \times 512 \times 568$, 2 artery seeds and 2 vein seeds were required along with 10 separator seeds. The separator seeds are required at few places where the structures are morphologically inseparable. We have compared our segmentation result with the ground truth data from [21] and presented in Table 1. Also we have the result with two direct predecessor methods of MSO-GP, i.e. Optimal erosion and IRFC. MSO-GP outperforms them in terms of all the evaluation parameters. To generate a vessel cast data, the animal was first exsanguinated. While maintaining ventilation at low PEEP, the pulmonary vasculature was flushed with 1L 2% Dextran solution and pneumonectomy was performed. While keeping the lungs inflated at approximately 22 cm H_2O Pawy, a rapid hardening methyl methacrylate compound was injected into the vasculature to create a cast of the pulmonary arterial and venous trees. The casting compound was mixed with red oil paint for the venous (oxygenated) side and blue oil paint for the arterial (deoxygenated) side of the vascular beds. The arterial side was also contrast-enhanced by the addition of 10 cc of Ethiodol to the casting compound. The vessel cast was scanned in a Siemens sensation 64 MDCT scanner with the following protocol: 100 mAs, 120 kV, pitch of 1 mm slice collimation;reconstruction: Siemens B30f kernel, 0.5 mm slice thickness, matrix and 0.47 mm pixel size. Due to partial volume effect in the MDCT image, true A/V separation by thresholding using a suitable CT value results in erroneous A/V segmentation. In our work, the effect of distinguishing contrast between A/V trees is eliminated.

Qualitative performance of the MSO-GP algorithm on the A/V tree extracted from human lung CT image is presented in Fig. 4. The thoracic region was imaged using a Siemens Sen- sation 64 multidetector CT scanner at 120 kVp and 100 mA. The subject was scanned in feet-first

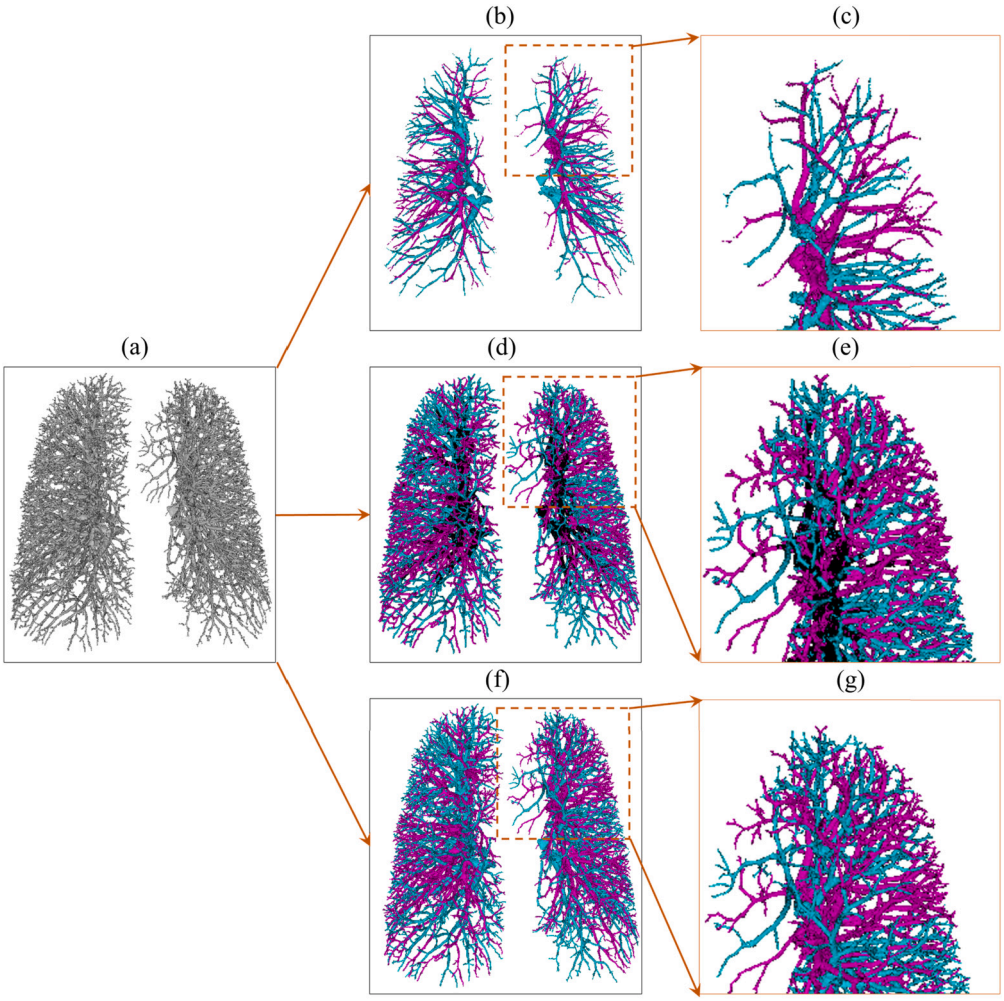

Fig. 5. Comparison of different methods (a) Original A/V tree of human lung. (b) Result of applying optimal erosion, many parts are missed. (c) Zoomed in view of the selected ROI from b. (d) Result of applying Iterative fuzzy connectivity, some parts are undecided (shown in black). (e) Zoomed in view of the selected ROI from d. (f) Result of applying MSO-GP. (g) Zoomed in view of the selected ROI from f.

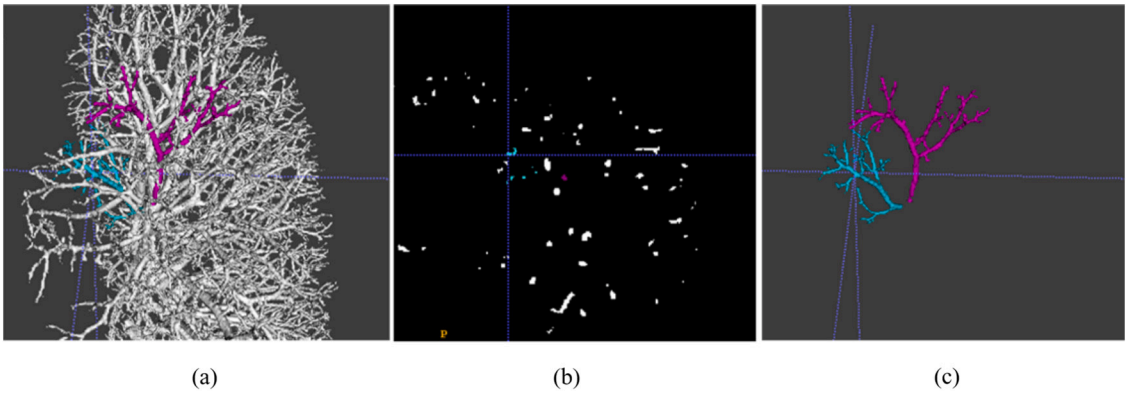

Fig. 6. Benchmarking and ground truth generation for separation of artery-vein in a small portion of Human Lung (a) Original Human Lung phantom with one annotated artery tree and one annotated vein tree, (b) Axial view of the A/V tree, where our annotated arteries and veins. (c) 3-D rendering of the annotated A/V tree.

supine position at full inspiration. CT protocol that obtains isotropic submillimeter images of the entire lung at total lung capacity has been used. The image was acquired at 0.75 mm slice thickness and was reconstructed with 0.5 mm slice thickness and $(0.55\ \text{mm})^2$ in-plane resolution [14]. The dimension of the human lung image is $512 \times 512 \times 667$. Domain experts took around 20 minutes for marking 15 artery seeds, 12 vein seeds and 10 separator seeds. Our algorithm produced output in just 6 minutes time. It is time consuming and tedious for a human expert to create ground truth segmentation for the whole human lung A/V tree because of its complex structure and orientation. Here a very small part of the human lung A/V tree was marked by expert with the help of ITK-SNAP paint brush tool. 4500 voxels were marked as artery or vein, an illustration of this process is provided in Fig. 6. Table 2 presents the quantitative performance of MSO-GP algorithm on human lung data

Table 1
Performance of MSO-GP on Pig Lung and comparison with two competing methods, Optimal erosion(OE) and Iterative relative fuzzy connectivity (IRFC), in terms of Precision (Pre), Recall (Rec), F1 score (F1), and Accuracy (Acc).

Methods	Pre	Rec	F1	Acc
MSO-GP	0.9583	0.9948	0.9762	0.9666
OE [21]	0.8943	0.6264	0.737	0.657
IRFC [22]	0.9326	0.8278	0.877	0.8362

Table 2
Performance of MSO-GP on Human Lung and comparison with two competing methods, Optimal erosion(OE) and Iterative relative fuzzy connectivity (IRFC), in terms of Precision (Pre), Recall (Rec), F1 score (F1), and Accuracy (Acc).

Methods	Pre	Rec	F1	Acc
MSO-GP	0.9498	0.9864	0.9678	0.9547
OE [21]	0.8514	0.5146	0.641	0.474
IRFC [22]	0.9054	0.8478	0.876	0.8062

and it outperforms two of its direct predecessor methods in terms of all the evaluation parameters. Our algorithm outperforms [23] in terms of execution time with less user intervention for both pig lung and human lung which establishes the superiority of our approach. In [24], the author presented a autmoatic pulmonary artery-vein separation from non-contrast CT scan images using tree partitioning and peripheral vessel matching. However the source code and CARVE challenge dataset used in the paper is not available in the public domain for comparison of the result. The authors in [25], presented a deep learning based method pulmonary artery-vein classification from non-contrast lung CT scan images. The source code and dataset used in this paper is also not publicly available for comparison of result.

In Fig. 5, we compare the performance of the proposed MSO-GP algorithm with two competing methods, one is optimal erosion and the other is iterative relative fuzzy connectivity (IRFC) [22]. For optimal erosion, we choose a 3x3x3 erosion operator which disconnects the conjoined arteries and veins. From Fig. 5(b), we can see the finer details are lost and only core arteries and veins are survived. Fig. 5(c) shows the result of applying IRFC where we can see many black spots which are undecided regions. Finally in Fig. 5(d), we can see the result of applying MSO-GP which is more comprehensive and robust than the other two. Please note that the experimental results shown in Fig. 4 and Fig. 5 are on two different human lung images, as is evident visually as well.

4. Conclusion

This work delves deeper into the classic computer vision problem of segmentation of complex conjoined structure with intertwined iso-intensity objects. Instead of blindly using a black box deep learning model, we investigate this challenge with a topological geometry and morphometric lens to provide a mathematical insight into the solution. To achieve this, we first applied a skeleton guided FDT based geodesic path propagation algorithm to generate object specific seeds and then applied the traditional MSO method that operates at multiple scales to separate the conjoined complex tree like large structures. We envision such an unsupervised analytical approach to be of particular interest to the discerning reader, as it provides some interpretable insights into the process compared to a purely data driven deep learning models. Moreover, such a model becomes indispensable for applications where we encounter large structure in size, but few in number, which poses a hard problem for learning algorithms. This is often the case in computational biology and to demonstrate this, we have chosen for our experimental validation, the task of iso-intensity artery-vein segmentation from low-contrast computed tomography lung angiograms. Our MSO-GP algorithm gives encouraging results on synthetic generated data, pig lung phantom data and human *in vivo* lung data. It also outperforms two competing methods. In this work, MSO-GP is applied to binary A/V tree to further separate them into arteries and veins. In future, MSO-GP can be extended to directly work with grey scale pulmonary CT images to separate arteries and veins. The basic assumption of MSO-GP algorithm is that the structures are morphologically separable but at few it may not hold. If structures are not morphologically separable then more object specific seeds/separators are required. MSO-GP implicitly used fuzzy connectivity as the main building block for separating structures. In future, we may replace fuzzy connectivity with better alternatives to overcome the morphological separability issue. MSO-GP algorithm may also be applied to other segmentation tasks like dendritic spine segmentation from microscopic images [26].

Code availability

The source code of MSO-GP can be found at: https://github.com/CMATERJU-BIOINFO/MSO-GP.

Declaration of competing interest

The authors declare that they have no known competing financial interests or personal relationships that could have appeared to influence the work reported in this paper.

Data availability

The data that has been used is confidential.

Acknowledgements

This work is partially supported by the CMATER research laboratory of the Computer Science and Engineering Department, Jadavpur University, India. Subhadip Basu acknowledges Department of Biotechnology grant (BT/PR16356/BID/7/596/2016) along with Science and Engineering Research Board, grant (SUR/2022/002903), Government of India. Tapabrata Chakraborti is supported by the Turing-Roche Strategic Partnership.

References

[1] N.O. Mahony, S. Campbell, A. Carvalho, S. Harapanahalli, G. Velasco-Hernandez, L. Krpalkova, D. Riordan, J. Walsh, Deep learning vs. traditional computer vision, arXiv:1910.13796.
[2] Z. Gao, R.W. Grout, C. Holtze, E.A. Hoffman, P.K. Saha, A new paradigm of interactive artery/vein separation in non-contrast pulmonary ct imaging using multi-scale topo-morphologic opening, IEEE Trans. Biomed. Imaging 59 (11) (2012) 3016–3027.
[3] C.M. van Bemmel, L.J. Spreeuwers, M.A. Viergever, W.J. Niessen, Level-set-based artery-vein separation in blood pool agent ce-mr angiograms, IEEE Trans. Med. Imaging 22 (10) (2003) 1224–1234.
[4] T. Lei, J.K. Udupa, P.K. Saha, D. Odhner, Artery-vein separation via mra-an image processing approach, IEEE Trans. Med. Imaging 20 (8) (2001) 689–703.
[5] T. Buelow, R. Wiemker, T. Blaffert, C. Lorenz, S. Renisch, Automatic extraction of the pulmonary artery tree from multi-slice CT data, in: Medical Imaging 2005: Physiology, Function, and Structure from Medical Images, vol. 5746, SPIE, 2005, pp. 730–740.
[6] T. Yonekura, M. Matsuhiro, S. Saita, M. Kubo, Y. Kawata, N. Niki, H. Nishitani, H. Ohmatsu, R. Kakinuma, N. Moriyama, Classification algorithm of pulmonary vein and artery based on multi-slice CT image, in: Medical Imaging 2007: Computer-Aided Diagnosis, vol. 6514, SPIE, 2007, pp. 754–761.
[7] P.K. Saha, S.A. Nadeem, A.P. Comellas, A survey on artificial intelligence in pulmonary imaging, Wiley Interdiscip. Rev. Data Min. Knowl. Discov. 13 (6) (2023) e1510.
[8] H. Li, Z. Tang, Y. Nan, G. Yang, Human treelike tubular structure segmentation: a comprehensive review and future perspectives, Comput. Biol. Med. 151 (2022) 106241.
[9] L. Xia, H. Zhang, Y. Wu, R. Song, Y. Ma, L. Mou, J. Liu, Y. Xie, M. Ma, Y. Zhao, 3d vessel-like structure segmentation in medical images by an edge-reinforced network, Med. Image Anal. 82 (2022) 102581.

[10] G. Tetteh, V. Efremov, N.D. Forkert, M. Schneider, J. Kirschke, B. Weber, C. Zimmer, M. Piraud, B.H. Menze, Deepvesselnet: vessel segmentation, centerline prediction, and bifurcation detection in 3-d angiographic volumes, Front. Neurosci. 14 (2020) 592352.
[11] F. Fu, J. Wei, M. Zhang, F. Yu, Y. Xiao, D. Rong, Y. Shan, Y. Li, C. Zhao, F. Liao, et al., Rapid vessel segmentation and reconstruction of head and neck angiograms using 3d convolutional neural network, Nat. Commun. 11 (1) (2020) 4829.
[12] Y. Qin, H. Zheng, Y. Gu, X. Huang, J. Yang, L. Wang, F. Yao, Y.-M. Zhu, G.-Z. Yang, Learning tubule-sensitive cnns for pulmonary airway and artery-vein segmentation in ct, IEEE Trans. Med. Imaging 40 (6) (2021) 1603–1617.
[13] J. Pu, J.K. Leader, J. Sechrist, C.A. Beeche, J.P. Singh, I.K. Ocak, M.G. Risbano, Automated identification of pulmonary arteries and veins depicted in non-contrast chest ct scans, Med. Image Anal. 77 (2022) 102367.
[14] P.K. Saha, Z. Gao, S.K. Alford, M. Sonka, E.A. Hoffman, Topomorphologic separation of fused isointensity objects via multiscale opening: separating arteries and veins in 3-d pulmonary CT, IEEE Trans. Med. Imaging 29 (3) (2010) 840–851.
[15] P.K. Saha, F.W. Wehrli, B.R. Gomberg, Fuzzy distance transform: theory, algorithms, and applications, Comput. Vis. Image Underst. 86 (3) (2002) 171–190.
[16] D.B. Johnson, A note on Dijkstra's shortest path algorithm, J. ACM 20 (3) (1973) 385–388.
[17] A.C. Jalba, J. Kustra, A.C. Telea, Surface and curve skeletonization of large 3d models on the gpu, IEEE Trans. Pattern Anal. Mach. Intell. 35 (6) (2012) 1495–1508.
[18] P.K. Saha, D. Jin, Y. Liu, G.E. Christensen, C. Chen, Fuzzy object skeletonization: theory, algorithms, and applications, IEEE Trans. Vis. Comput. Graph. 24 (8) (2017) 2298–2314.
[19] P.A. Yushkevich, Y. Gao, G. Gerig, Itk-snap: an interactive tool for semi-automatic segmentation of multi-modality biomedical images, in: 2016 38th Annual International Conference of the IEEE Engineering in Medicine and Biology Society (EMBC), IEEE, 2016, pp. 3342–3345.
[20] A. De, N. Das, R. Sarkar, P.K. Saha, S. Basu, Design of synthetic 3-d pulmonary phantoms using 2-d graphical user interface, in: International Conference on Computational Intelligence, Communications, and Business Analytics, Springer, 2018, pp. 223–233.
[21] P.K. Saha, S. Basu, E.A. Hoffman, Multiscale opening of conjoined fuzzy objects: theory and applications, IEEE Trans. Fuzzy Syst. 24 (5) (2015) 1121–1133.
[22] K.C. Ciesielski, J.K. Udupa, P.K. Saha, Y. Zhuge, Iterative relative fuzzy connectedness for multiple objects with multiple seeds, Comput. Vis. Image Underst. 107 (3) (2007) 160–182.
[23] P.K. Saha, S. Basu, E.A. Hoffman, Multiscale opening of conjoined fuzzy objects: theory and applications, IEEE Trans. Fuzzy Syst. 24 (5) (2016) 1121–1133, https://doi.org/10.1109/TFUZZ.2015.2502278.
[24] J.-P. Charbonnier, M. Brink, F. Ciompi, E.T. Scholten, C.M. Schaefer-Prokop, E.M. Van Rikxoort, Automatic pulmonary artery-vein separation and classification in computed tomography using tree partitioning and peripheral vessel matching, IEEE Trans. Med. Imaging 35 (3) (2015) 882–892.
[25] P. Nardelli, D. Jimenez-Carretero, D. Bermejo-Pelaez, G.R. Washko, F.N. Rahaghi, M.J. Ledesma-Carbayo, R.S.J. Estépar, Pulmonary artery–vein classification in CT images using deep learning, IEEE Trans. Med. Imaging 37 (11) (2018) 2428–2440.
[26] S. Basu, P.K. Saha, M. Roszkowska, M. Magnowska, E. Baczynska, N. Das, D. Plewczynski, J. Wlodarczyk, Quantitative 3-d morphometric analysis of individual dendritic spines, Sci. Rep. 8 (1) (2018) 3545.